The generation of prograde P–T–t points and paths; a textural, compositional, and chronological study of metamorphic monazite

G. Foster[a],[*], R.R. Parrish[b],[c], M.S.A. Horstwood[c], S. Chenery[d], J. Pyle[e], H.D. Gibson[f]

[a]Department of Earth Sciences, Wills Memorial Building, University of Bristol, Queens Road, Bristol, BS8 1RJ, UK
[b]Department of Geology, University of Leicester, University Road, Leicester, LE1 7RH, UK
[c]NERC Isotope Geosciences Laboratory, British Geological Survey, Nottingham, NG12 5GG, UK
[d]British Geological Survey, Nottingham, NG12 5GG, UK
[e]Department of Earth and Environmental Sciences, Rensselearer Polytechnic Institute, Troy, NY 12180-3502, USA
[f]Department of Geosciences, University of Massachusetts, Amherst, MA 01003, USA

Abstract

Analogue and computational models principally provide our present understanding of the mechanisms of prograde metamorphism and orogenesis, yet, due to the difficulty of linking prograde age information with the pressure–temperature (P–T) evolution of a rock, these models for the most part remain untested. Here, we describe an approach that allows multiple prograde pressure–temperature–time (P–T–t) points to be generated on single samples providing a means to construct detailed P–T–t loops, enabling the duration of metamorphic events, the timing of burial and the rate of heating experienced by individual samples to be determined. We use this combination approach to generate multiple prograde P–T–t points for three samples from the Himalayan and Canadian Cordillera and show for the first time that the duration of the metamorphic events are similar in each area and prograde heating rates vary from 2.4±1.2 °C/Ma to 5.0±2.0 °C/Ma. The P–T–t paths generated this way agree well with the established geological history of the studied areas and allow additional constraints to be placed on the mechanisms of orogenesis.
© 2004 Elsevier B.V. All rights reserved.

Keywords: monazite; geochronology; U–Pb; laser ablation; geothermobarometry; P–T–t paths

* Corresponding author. Tel.: +44 117 954 5235; fax: +44 117 925 3385.
E-mail addresses: G.L.Foster@Bristol.ac.uk (G. Foster), rrp@nigl.nerc.ac.uk (R.R. Parrish), mash@bgs.ac.uk (M.S.A. Horstwood), srch@bgs.ac.uk (S. Chenery), pylej@rpi.edu (J. Pyle), gibson@geo.umass.edu (H.D. Gibson).

1. Introduction

Central to our understanding of orogenic processes is an appreciation of the timescales over which these processes operate. Knowledge of such time information has increasingly been one of the goals of

geochronology. For orogenesis, the timing and nature of exhumation that accompanies, and often signals the termination of, an orogenic event is well characterised but the initial timescales of prograde metamorphism accompanying the earlier stages of orogenesis are poorly constrained. To date, few studies provide quantitative estimates of orogenic heating and burial rates (see review by Vance et al. [1]). Instead, much of our understanding of the processes involved in prograde orogenesis comes from analogue and computational modelling [2–4]. These models, for the most part, remain untested due to the paucity of data on the timescales of prograde metamorphism.

Here, we outline a methodology, utilising recent advances in both accessory mineral chronology and thermobarometry, which allows the ready determination of prograde temperature–time (T–t) and pressure–time (P–t) points. Previously, such prograde pressure–temperature–time (P–T–t) information could only be generated through analytically arduous techniques, such as the radiometric dating of garnet (e.g., [5]). Although successful, these approaches have only a limited applicability (e.g., only samples with sufficiently large garnets can be separated into the core-rim separates required to date initial garnet growth) and suffer from a number of complications (e.g., [6]). The approach followed here involves the in situ dating of compositionally distinct portions of metamorphic monazite using laser ablation multi-collector inductively coupled plasma mass spectrometry (LA-MC-ICPMS). Recent advancements in accessory mineral thermobarometry now allow accurate and precise estimates of the temperature to be determined at which various portions of monazite grew [7,8]. Pressure constraints are more elusive, but an approach involving textural studies and petrogenetic grids now allows approximate pressure information to be generated in some cases [9]. A combination of these novel techniques allows the generation of prograde P–T–t paths with few of the analytical challenges that accompanies rock-forming mineral chronology.

In this study, we begin by placing absolute and relative P–T constraints on monazites in three samples from the recent Himalayan and the Canadian Cordilleran orogens, which we interpret using the textural study detailed in [10]. We then place these P–T constraints in a temporal framework by carrying out a number of new in situ LA-MC-ICPMS U–Pb analyses, in thin sections of the studied samples, significantly augmenting their existing chronology [10]. By following this approach, we are able to generate P–T–t points for multiple portions of individual monazite crystals, enabling a thorough reconstruction of the prograde P–T–t history of each sample. This allows us to establish for the first time that the duration of metamorphic events and heating rates are similar in both orogens (20–30 million years and 2–5 °C/Ma).

2. Geological setting

The samples for this study come from the Cretaceous–Tertiary Himalayan and Canadian Cordilleran orogenic zones. Samples DG167 and DG136 are from the Monashee complex of the Canadian Cordillera, an amphibolite facies footwall structurally overlain by an allochthon of upper amphibolite facies crustal rocks. Samples DG136 and DG167 crop out ~600 m and 2.1 km below the Monashee Decollement, the roof thrust for the Monashee Complex [11].

Sample K98-6 comes from the sillimanite-zone rocks structurally below the Hunza Plutonic Unit of the Hunza Valley, Pakistan (see [12]), within the hanging wall of the Shyok Suture zone and Main Mantle Thrust that comprise the Indian–Asian structural boundary. In both areas, metamorphism is thought to have occurred during collisional orogenesis. The reader is referred to [11,12] for more detailed descriptions of the sample locations.

3. Sample descriptions

Samples DG167 and DG136 are both amphibolite facies pelitic schists with assemblages of quartz, plagioclase, muscovite, biotite, garnet, kyanite, and with accessories of rutile, opaques, monazite, zircon, xenotime, allanite, and apatite. Sample DG136 also contains sillimanite (fibrolite) and K-feldspar, probably growing via muscovite breakdown at or near peak P–T. Sample K98-6 is a sillimanite-bearing metapelite that contains leucocratic segregations and has an assemblage of quartz, garnet, plagioclase, sillimanite, and biotite, with accessories of monazite, zircon,

apatite and graphite. The restitic portion of K98-6 has a similar assemblage but with subordinate amounts of quartz, plagioclase and K-Feldspar. Peak P–T estimates determined using average P–T mode of the computer program THERMOCALC v. 2.75 [13] indicate that sample DG136 reached a peak P–T of 728±24 °C and 10.2±1.2 kbar, sample DG167 reached a peak of 665±23 °C and 8.8±1.1 kbar, and sample K98-6 reached a peak of 653±110 °C and 5.5±1.8 kbar [9]. Using conventional garnet–biotite thermometry [14] the peak temperatures for these samples are 725, 705 and 635 °C, respectively (Foster, unpublished data).

4. Methodology and approach

Monazite is the mineral of choice for dating amphibolite grade metamorphism (e.g., [15]), yet unlike rock-forming minerals, such as garnet, it has been difficult to link monazite age information to P–T information in metamorphic rocks. This situation has been ameliorated recently by two approaches, both of which will be followed here. In the first, the growth history of accessory minerals are related to the growth history of rock-forming minerals through textural observations, such as the identification of inclusion relationships. By placing the reaction history of the rock-forming minerals into a P–T framework using P–T pseudosections (e.g., [16]), constraints can be placed on the growth P–T for monazite (for a complete review of this approach, see [9]). The second approach places more absolute constraints on the temperature of monazite growth utilising the recent calibrations of a garnet–monazite thermometer [8] and a monazite–xenotime thermometer [7,17]. The methodology followed here is similar to that outlined in [8]. A common feature of metamorphic monazite is that it is often complexly zoned in yttrium, a feature that is related to the episodic growth of monazite during a single metamorphic event at different P–T conditions (e.g., [10,18,19]). Using these two thermobarmetric approaches, each monazite zone can be assigned a P–T, such that in most instances, a single crystal can record two or three P–T points.

In order to exploit the P–T information contained in metamorphic monazite, an in situ dating technique must be used that allows the textural context of the

Table 1
Summary of accessory phase relationships and compositions

	Sample		
	K98-6	Dg136	Dg167
Accessory phases[a]			
Mnz[b]	x	x	x
Aln		x	x
Xen	x	x	x
Zrn	x	x	x
Tho[c]			
Ap	x	x	x
Accesory phase relationships[d]			
Grt	Mnz, Xen	Mnz[r], Aln[co]	Mnz[r], Aln[co]
Kyn	O	Mnz[r], Aln[co]	Aln
Matrix	Mnz, Xen[br]	Mnz, Xen[br]	Mnz, Xen[br]
Monazite textures[e]			
Zone-1	Cores of matrix grains, inclusions in grt	Cores of matrix and grains included in grt and kyn	Cores of matrix grains inclusions in grt
Zone-2	Inner rims of matrix grains, outer rim of inclusions	Outer rim of grains in kyn inner rim of matrix grains	Outer rims of matrix grains, absent from inclusions
Zone-3	Outer rim of matrix grains, absent from inclusions	Outer rim of matrix grains	
Zone-4	Rare appendage (?) like growths on grain rims		
Monazite composition (Y_2O_3 wt.%)[f]			
Zone-1	1.9–2.8	0.1–0.4	0.4–0.8
Zone-2	1.0–1.4	1.2–1.6	0.9–1.1
Zone-3	1.8–1.9	2.1–2.7	
Zone-4	<1.9		

[a] An x denotes that the accessory phase was observed in the sample.
[b] Mineral abbreviations as [47] plus Tho=thorite, Mnz=monazite, Aln=allanite, Xen=xenotime, Zrn=zircon.
[c] Also grouped here are Th-phosphates.
[d] Summary of accessory phase textural relationships. An "o" indicates pophyroblast phase is absent; "br" indicates phase is related to the breakdown of garnet; "co" indicates accessory phase occurs only as an inclusion in the core of porphyroblast phase; "r" indicates accessory phase only occurs as an inclusion in the rim of the porphyroblast phase. Matrix row lists which phases are stable in the matrix.
[e] Textural characteristics of monazite. Each zone has a distinct Y-composition and they are listed in relative age order.
[f] Monazite Y content determined by EMP (see [9,10]).

monazite to be retained and it must be spatially precise enough to target individual monazite growth zones (which are often less than 20 μm wide). In this contribution, we use the newly developed laser ablation multicollector inductively coupled mass spectrometry technique to date monazite using the U–Pb system in petrographic thin section. The full methodology of this approach is outlined in [20].

5. Monazite textural and compositional characteristics

Critical to this study are the textural (i.e., inclusion relationships) and compositional characteristics of the accessory minerals monazite, xenotime, and allanite. Accessory mineral textures and monazite compositional variability in these samples have been discussed
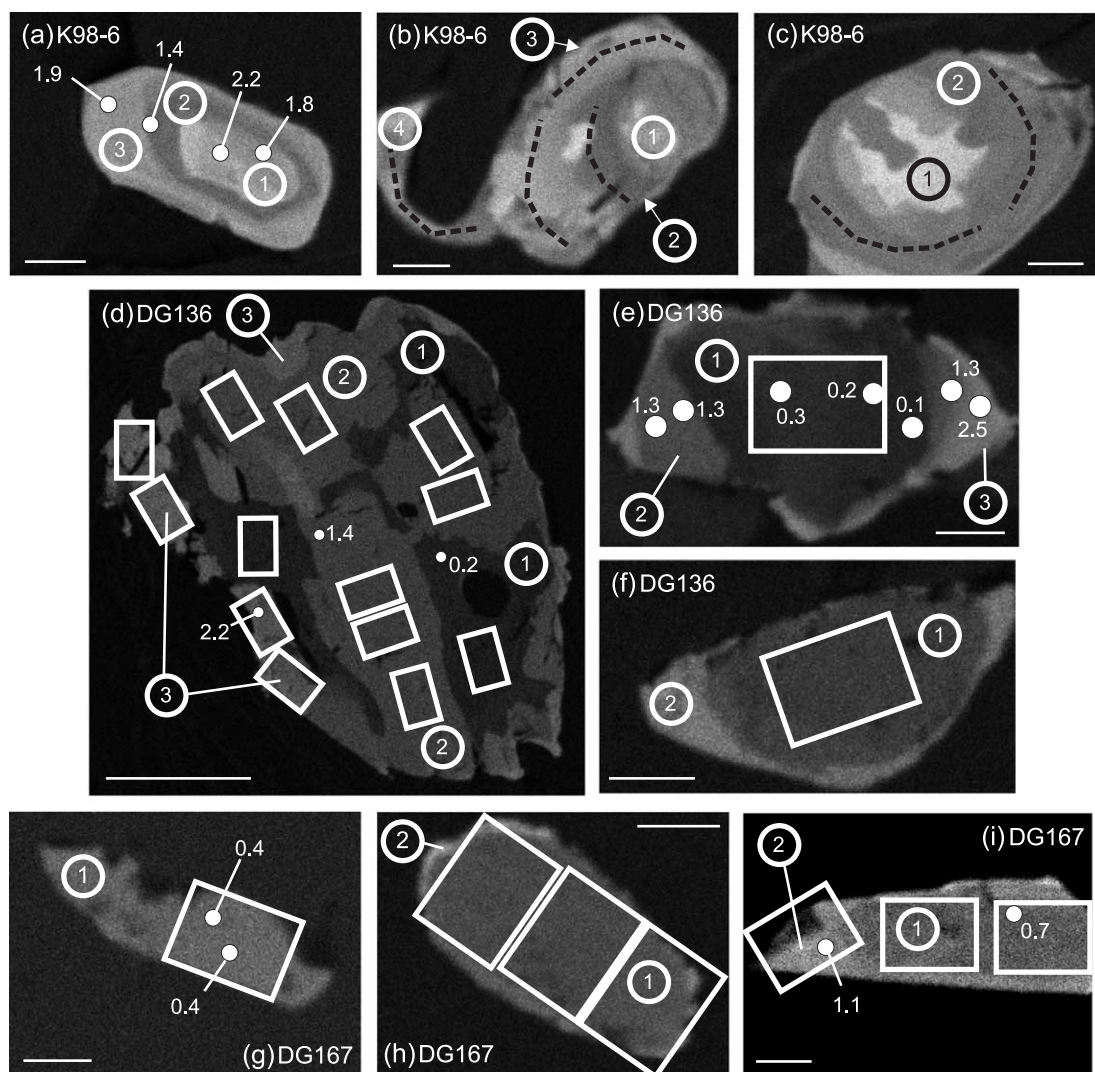

Fig. 1. X-Ray maps of Y content in selected monazites from K98-6 (a, b, and c), DG136 (d, e, and f) and DG167 (g, h, and i). In all cases, Y content is proportional to grey-scale intensity. Note that grey-scale has been manipulated so it is not necessarily comparable between images. White spots show the location of EMP analyses, labelled according to Y_2O_3 wt.%. Rectangles show the location of LA-MC-ICPMS box raster analyses, black dotted lines show the location of LA-MC-ICPMS line rasters. The monazite zones are labelled 1 to 4 (numbers in circles), see Table 1 and text. The scale bar is 20 μm in all images except (d) where it is 100 μm.

in detail in [10] and are summarised in Table 1. Monazites in all three samples exhibit limited zoning of Th and U but large variations of Y content are common (Figs. 3, 4, 6 and Table 2 in [10], Fig. 1). A number of zones with distinct Y composition can be identified and each zone can be assigned a relative age (labelled zone-1 to zone-4). This analysis is summarised in Fig. 1 and Table 1.

6. Garnet composition

Garnet is an essential mineral in both the conventional determination of P–T and the two approaches applied in this contribution. In order to correctly apply the garnet–monazite thermometer and to aid the interpretation of monazite Y zoning, an understanding of the reaction history and compositional variation of garnet (especially Y) is vital. The compositional variations exhibited by the garnets in the three samples investigated here are illustrated in Fig. 2. Electron microprobe operating conditions are detailed in the figure caption for Fig. 2. Quantitative trace element and REE analysis of these garnets, guided by the X-ray maps, was carried out using LA-ICPMS at the British Geology Survey, following the methodology outlined in [21]. Because a full discussion of the REE and trace element variation in these garnets is beyond the scope of this contribution, only the Y contents of the examined garnets will be considered here (listed in Table A1 in the EPSL online background data set, associated with this contribution).

In all three samples, garnet is a porphyroblast phase that varies from <5 mm (K98-6) to ~1 cm (DG136) in diameter. In samples K98-6 and DG136, major element zoning is only weakly developed (Fig. 2b, c, and e) and has probably been homogenised by diffusion at elevated temperatures. In contrast, DG167 displays relatively strong major element zoning typical of growth zoning (Fig. 2i and j; [22]). Retrograde diffusional exchange with matrix biotite, evident as an increase in Fe and Fe/(Fe+Mg) in the rims of garnet, is present in all three samples. Also evident are textures indicative of garnet breakdown, a situation that is consistent with the observed increase in Mn at the rims of all the garnets.

Garnets in sample K98-6 display strong core-rim zoning in Y, with a relatively homogeneous core

with ~500 ppm Y and a rim with ~100–200 ppm Y (Fig. 2a–c). The transition between the two zones is abrupt and, according to [23], is indicative of garnet growth coincident with the consumption of reactant xenotime. In this model, the high-Y core grew in equilibrium with xenotime whereas the rim grew following its exhaustion. The sharp transition zone illustrates the rapidity with which Y is partitioned into garnet through a Rayleigh fractionation process [23]. Xenotime was observed included in the core region of one of the six garnets studied. Application of the xenotime–garnet thermometer of [24] indicates the cores of these garnets grew at ~550 °C.

In samples DG136 and DG167, Y displays very little zoning in garnet and the average Y content is ~90 and ~60 ppm, respectively (Fig. 2d and h; Table A1 in the EPSL online background data set). In both samples, Y content increases towards inclusions of quartz and feldspar (Fig. 2d, g, and h), locally reaching ~600–700 ppm. In sample DG136, there is one, possibly two, annuli of high Y (Fig. 2d and f) where the Y content increases to ~400 ppm. According to [23], Y annuli in garnet indicate a period of garnet regrowth, subsequent to garnet resorbtion, for example, during staurolite growth. Alternative mechanisms for the development of such annuli are discussed in [25]. The elevated Y around inclusions may reflect the sites of initial garnet nucleation or preferential replacement of low-Y garnet by later high-Y garnet along localised fluid pathways.

Critical for the accurate application of the garnet–monazite thermometer is an understanding of which phase of garnet grew in equilibrium with which monazite zone. For sample DG136, an important observation is that monazite is only found rimward of the Y-annuli, included in low-Y garnet. Similarly for sample DG167, monazite is found only included in low-Y garnet.

7. Monazite petrogenesis and reaction history

By utilising the textural relationships of monazite and xenotime, the compositional information outlined previously, and the guidelines listed in [9], we have been able to deduce the reaction history and petrogenesis of monazite in these samples. There are
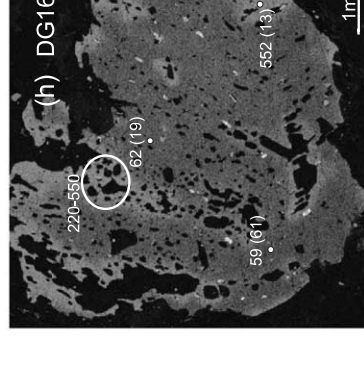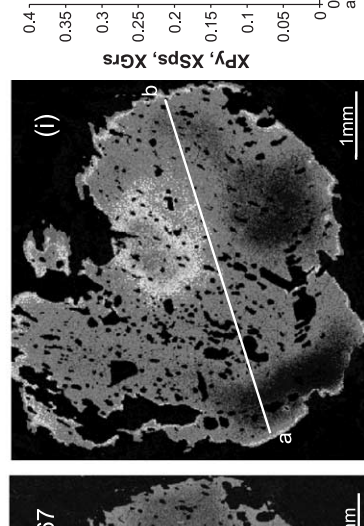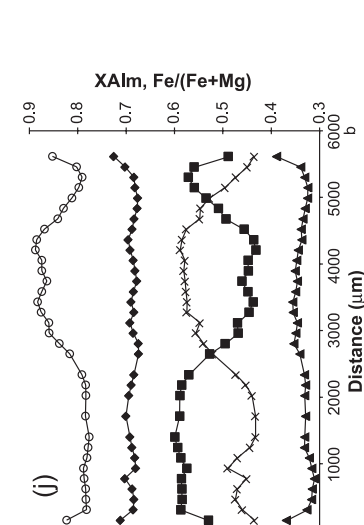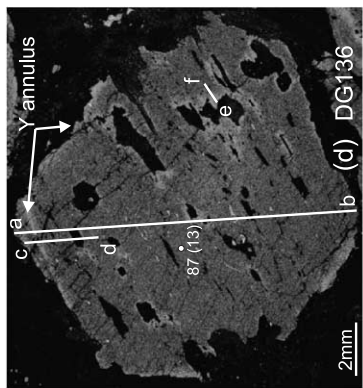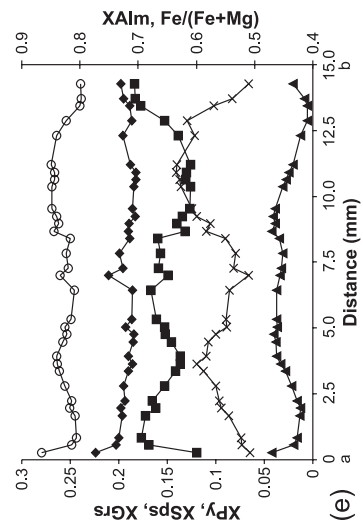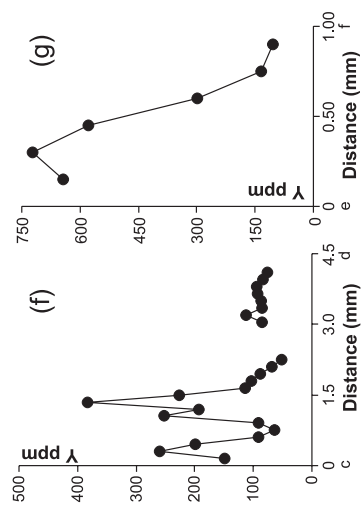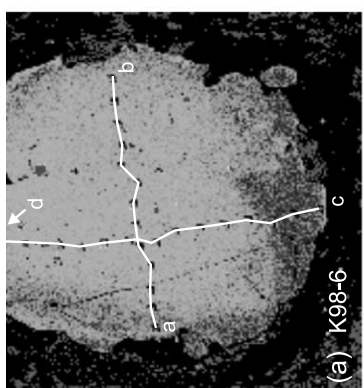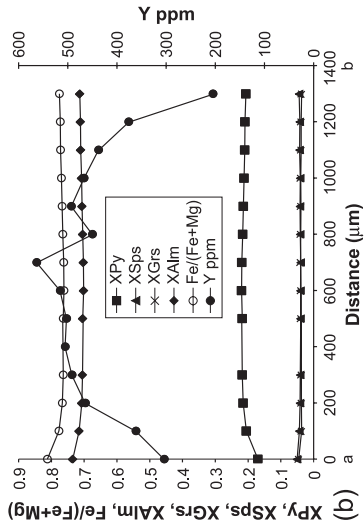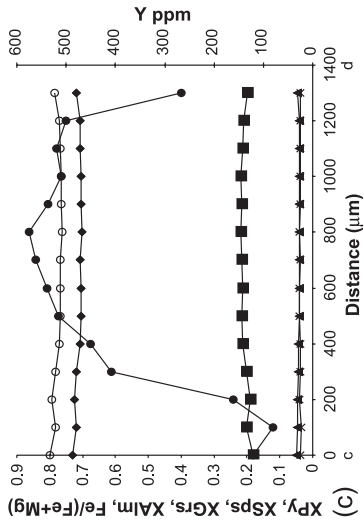
several key observations and interpretations, and these are summarised below.

7.1. K98-6

(1) Four zones of monazite growth can be identified on the basis of Y content (Fig. 1, Table 1).
(2) Zone-1 monazite is included in garnet. This texture, in addition to its relatively high Y content, indicates this monazite either grew before garnet had entered the assemblage or, if it grew at the same time as the occluding garnet, both phases were in equilibrium with xenotime [8,9].
(3) Garnet has a relatively high-Y core (~500 ppm) and low-Y rim (~150 ppm; Fig. 2a), suggesting only the high-Y core grew in equilibrium with xenotime (cf. [23]). It is therefore likely that zone-1 monazite grew in equilibrium with the high-Y garnet core (if it grew in equilibrium with garnet at all).
(4) Zone-3 is absent from monazites included in garnet. This observation suggests this phase grew after garnet had grown. Since early garnet growth would have sequestered most of the available Y [23], the high Y content of this zone indicates it grew during garnet breakdown when the Y content of the effective bulk composition would have increased [9]. This portion of monazite is likely to be in equilibrium with matrix xenotime that grew as a consequence of garnet breakdown [9].
(5) Zone-2 therefore grew after prograde xenotime had left the assemblage and garnet growth had sequestered the available Y. Its low Y content suggests it grew during the growth of the low-Y garnet rim.

(6) Zone-4 is the last phase to grow, if it grew in equilibrium with matrix xenotime its low Y content suggests it grew at a relatively low temperature.

7.2. DG136

(1) Three zones of monazite can be identified on the basis of Y content (Fig. 1, Table 1).
(2) Monazite inclusions in garnet are rare and they are only present in the outermost (low-Y) rims of garnet (beyond the Y annuli; Fig. 2). Monazite is also included in kyanite, but allanite is included in the cores of both these phases. Since zone-1 is the first stage of monazite growth, these textures suggest this phase grew from allanite during the latter growth stages of garnet and during the growth of kyanite.
(3) The last phase of monazite growth is zone-3, which has a relatively high Y content (~2.5 wt.% Y_2O_3). Following an argument similar to that made above for K98-6 zone-3, this last phase of monazite growth occurred during garnet breakdown and in equilibrium with matrix xenotime.
(4) Zone-2 is present in monazite included in kyanite (no inclusions in garnet were examined), but zone-3 is absent. Since zone-3 grew during garnet breakdown, zone-2 probably grew during prograde metamorphism, during the growth of kyanite and prior to the breakdown of garnet.

7.3. DG167

(1) Two stages of monazite growth can be identified in this sample on the basis of Y content (Fig. 1, Table 1).

Fig. 2. Garnet composition in samples K98-6 (a, b, and c), DG136 (d, e, f, and g) and DG167 (h, i, and j). (a), (d), and (h) are Y X-ray maps of garnet porphyroblasts in samples K98-6, DG136, and DG167, respectively. Grey-scale intensity is proportional to Y content. (i) Mn X-ray map of sample DG167, grey-scale intensity proportional to Mn content. (b), (c), (e), (f), (g), and (j) are line profiles showing mole fraction of Fe (diamonds; Almandine), Mn (triangles; Spessatine), Mg (squares; Pyrope) and Ca (crosses; Grossular) and the Fe/(Fe+Mg) ratio (open circles) in garnet. Also shown is Y in ppm (b, c, f, and g; filled circles). The location of the traverses are shown on their respective Y or Mn X-ray map. On maps (d) and (h), white spots show the location, mean Y content, and associated 2 S.D. of a number of LA-ICPMS analyses. The large open white circle on (h) shows an area multiply analysed labelled according to the observed range of Y (220–550 ppm). Major element analysis was performed at the University of Leicester using a JEOL 8600S electron microprobe (EMP) with a 15-kV accelerating voltage with a 30-nA probe current and focused electron beam. Major, trace, and rare earth element X-ray maps were collected at the Manchester University electron probe facility and the University of Bristol, using a Cameca SX100 EMP operating with a 20-kV accelerating voltage, a 2-μA probe current, a focused electron beam and at a resolution of 1024×1024 to 512×512 pixels with a 5–15 μm pixel spacing and 35 ms/pixel dwell time.

(2) The chemical composition of zone-1 (0.4 to 0.8 wt.% Y_2O_3) and monazites' first occurrence in the rims of garnet indicate this phase of monazite grew after garnet had entered the assemblage (in equilibrium with low-Y primary garnet) and after the exhaustion of prograde xenotime.

(3) The presence of allanite in the cores of garnets and in kyanites, but stable monazite in the matrix, indicates zone-1 grew after kyanite had entered the assemblage.

(4) Zone-2 has an elevated Y content (0.9 to 1.1 wt.% Y_2O_3) and is not found in inclusions in garnet; this zone may have grown in equilibrium with matrix xenotime following the break down of garnet. Alternatively, because the Y content of this zone is not significantly higher than zone-1 (Table 1), this monazite may simply have grown in equilibrium with garnet at a higher temperature.

8. P–T results

8.1. Pseudosections

P–T pseudosections were constructed for each sample in the MnCaNaKFMASH system following the methodology outlined in [16] using the computer program THERMOCALC v. 2.75 [13], the thermo-

dynamic database of [26] and the whole rock compositions shown in Table 3 of [10]. Complete pseudosections for all three samples are shown in, Fig. A1 in the EPSL online background data set, associated with this contribution; their relevant features are summarised in Fig. 3. For all samples, the observed matrix assemblage is predicted to be stable at the estimated peak P–T. In samples DG136 and K98-6, the garnet major element composition (Fig. 2) has been diffusionally homogenised, precluding the extraction of the P–T conditions of garnet growth (e.g., [16]). Nevertheless, a minimum estimate of the P–T of garnet growth in these two samples is
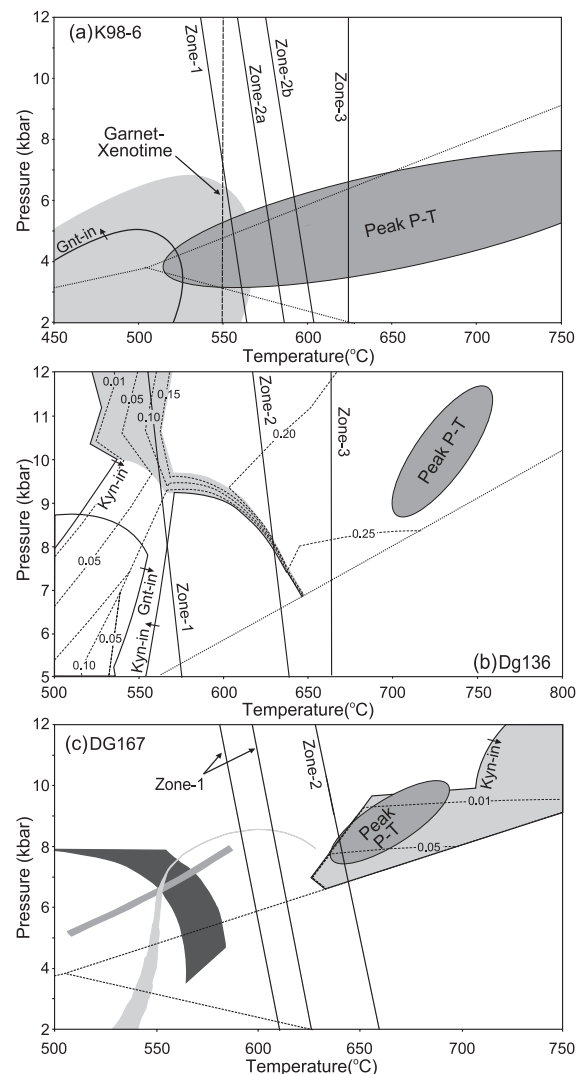

Fig. 3. A P–T summary diagram for (a) K98-6, (b) DG136, and (c) DG167. The dotted black lines in all plots are the Al_2SiO_5 polymorph stability boundaries. On all images, the dark grey ellipse shows the position of the peak P–T estimate determined by THERMOCALC. In panels (a), (b), and (c), the estimated conditions of monazite stability as determined by garnet–monazite thermometry are shown as black solid lines labelled with corresponding growth zone (1 to 3). Fields that provide constraints on monazite stability are shaded in light grey: in (a), the shaded field is the garnet absent field (with a small degree of overstep); in (b), the field where the majority of kyanite is growing (constructed using the whole rock composition with a garnet component removed) is shaded; in (c), the kyanite-bearing field is shaded. Kyanite modal abundance contours are shown in (b) and (c) as dashed lines. In (a) and (b), the garnet reaction line is shown and labelled; in (c), the measured composition of the garnet core is shown, the dark grey band is XMn=0.055, mid grey is XCa=0.185, light grey is XFe=0.68. In (a), the vertical dashed line is the temperature estimate from garnet–xenotime thermometery. In (b) and (c), the kyanite-in reaction line is shown and labelled. Mineral abbreviations are as [47].

given by the position of the garnet-in reaction line (Fig. 3). The garnet core of DG167 (taken as the highest Mn content measured; XMn=0.55, XCa=0.185, XFe=0.68) is predicted by THERMOCALC to occur at 559±10 °C and 6.9±0.3 kbar. The peak P–T conditions for all samples (Fig. 3) lie at higher pressures and temperatures than the estimates of initial garnet growth, suggesting metamorphism occurred during increasing P and T, i.e., during burial and subsequent thermal equilibration. Additional constraints are provided by the garnet modal abundance contours (Fig. A1 in the EPSL online background data set), which indicate that in all samples, garnet will only grow on such a P–T path. In addition, since kyanite is stable at higher pressures and temperatures than the estimates of garnet growth in samples DG167 and DG136, the presence of matrix kyanite is consistent with metamorphism on a path of increasing P–T. Semiquantitative constraints on the shape of the P–T path for sample DG167 are given by the Ca and Fe zoning in garnet. Fe shows little zonation (Fig. 2j) as would be expected if the P–T path followed the Fe contour lines (see Fig. 3c). Ca is flat in the core of the garnet (Fig. 2j) but then decreases rapidly. Ca decreases with increasing temperature (not shown), so this zoning pattern suggests the P–T path followed a Ca contour then perhaps evolved perpendicular to it. These constraints are used to construct the P–T for this sample shown in Fig. 5d. For sample K98-6, xenotime–garnet thermometry supports the growth of garnet at ~550 °C, ~100 °C lower than the peak temperature estimate.

For sample K98-6, the pseudosection places constraints on the P–T of zone-1 monazite. This monazite grew before, or at the same time as garnet, the P–T of initial garnet growth can be estimated from the pseudosection at a minimum of ~550 °C and <6 kbar (a minimum because of finite reaction overstep; Fig. 3). This temperature estimate is similar to that provided by xenotime–garnet thermometry of the garnet core, suggesting that the garnet core, and hence the zone-1 monazite did indeed grow at these conditions. If zone-2 monazite grew in equilibrium with the garnet rim, then the P–T of this phase is constrained by the previous estimate and the peak P–T (~630 °C and ~5.5 kbar).

In samples DG136 and DG167, monazite begins to grow from allanite during the growth of the garnet rims and during the growth of kyanite. In both samples, the majority of kyanite growth occurs from staurolite or chloritoid breakdown, and only a small amount grows once these phases have left the assemblage (Fig. A1 in the EPSL online background data set). In sample DG136, both allanite and monazite are found included in kyanite. Therefore, the first phase of monazite growth in this sample (zone-1) must have occurred during the growth of kyanite, and hence probably during staurolite/chloritoid breakdown. In order to overcome the affect garnet growth has upon the effective bulk composition (cf. [16,27]), the bulk composition at the time of monazite growth has been estimated. This was calculated using the observed modal abundance of garnet that contains allanite inclusions (~15 modal %) and the measured composition of garnet. The pseudosection constructed from this new composition is also shown in Fig. A1 in the EPSL online background data set and summarised in Fig. 3b. Notably, the kyanite stability field has not been greatly affected by the growth of garnet (cf. [27]). Using this pseudosection, we can constrain the P–T of the first phase of monazite growth in this sample to 520–650 °C and ≥7 kbar (i.e., the staurolite/chloritoid bearing fields where the majority of kyanite growth occurs; the shaded area in Fig. 3b). Zone-2 monazite is also present in kyanite, indicating that kyanite growth must have continued on the prograde path (providing a useful constraint on the shape of the P–T path). A best estimate for the P–T of this zone lies between the estimate for zone-1 and the peak P–T (728±24 °C and 10.2±1.2 kbar).

The scenario for sample DG167 is very similar and because allanite is included in kyanite (no monazite was observed included in kyanite), allanite, not monazite was stable during kyanite growth. Fig. 3c shows that kyanite only becomes stable at ≥6.6 kbar and ≥625 °C, i.e., quite close to the peak P–T. This is consistent with the observation that monazite (not allanite) is found included in the rims of garnet. Once staurolite leaves the assemblage, kyanite modal abundances decrease with increasing P–T, probably due to garnet growth (in the chlorite and staurolite absent fields garnet contours are inverse to and parallel those of kyanite, Fig. A1 in the EPSL online background data set). Zone-1 monazite growth must

have occurred sometime after the stability field of kyanite had been reached, 625 °C and 6.6 kbar are therefore minimum estimates of the P–T at which the first phase of monazite growth occurred in this sample (zone-1). An upper estimate is given by the peak P–T estimate of 665±23 °C and 8.8±1.1 kbar. As demonstrated for sample DG136, garnet growth does not seem to greatly affect the position of the kyanite stability field. We therefore believe this estimate is accurate, despite the fractionation of the bulk composition that would have occurred following the growth of garnet.

8.2. Monazite–xenotime thermometry

Following [8], only the high-Y rims of the matrix monazites of the samples examined here are assumed to be in equilibrium with matrix xenotime. In all three samples, matrix xenotime has grown because garnet has broken down to biotite/chlorite and quartz, and these phases do not contain appreciable amounts of Y, thus releasing Y to the effective bulk composition and stabilising xenotime [10,23]. The pseudosections for these samples (Fig. A1 in the EPSL online background data set) indicate that garnet will break down in all three samples on paths of decompression; thus, retrograde replacement of garnet and the growth of xenotime probably occurred during decompression following the attainment of peak P–T and on the retrograde portion of the P–T loop. Because of the nature of tectonic exhumation, it is likely that decompression and garnet breakdown occurred before cooling, due to the slow diffusion of heat in rock [28]. Therefore, the temperature given by the monazite–xenotime thermometer for high-Y rim monazite should closely relate to the peak P–T, provided sufficiently rapid exhumation [9]. Here, we use the thermometer of [7]. Similar results are obtained with the calibration of [8] (not shown here) but the estimates are lower than the experimental calibration of [17] for the reasons outlined in [19].

Table 2 shows the temperature estimates for the high-Y monazite rims of all three samples. For samples K98-6 and DG136, temperatures are close to, or within error of, the peak temperature determined by THERMOCALC and garnet–biotite thermometry (Section 3), placing accurate tempe-

Table 2
Accessory mineral thermometry

Sample	K98-6	Dg136	Dg167
	Peak temperatures (°C)		
Thermocalc	653±110	728±24	665±23
Grt-Bt[a]	632–638	721–729	698–705
Monazite–xenotime[b]			
	Zone-3	Zone-3	Zone-2
1	624 (6, 6)	663 (26, 8)	455 (86, 5)
2	676 (10, 6)	708 (73, 8)	271 (53, 5)
Monazite–garnet			
Zone-1			
T (°C)[c]	553	569	595–611
XYAG	0.000996	0.000147	0.000109
XGrs	0.0407	0.0707	0.085
XYMon	0.0532	0.007	0.007–0.01
Zone-2			
T (°C)[c]	575–592	632	643
XYAG	0.00021	0.000147	0.000109
XGrs	0.0385	0.0707	0.085
XYMon	0.0208–0.0313	0.03	0.02
XOH_{ap}[d]	0.25	0.25	0.25
f_{H2O}	5020	5020	5020
P (kbar)	6	7	7
XAn	0.36	0.27	0.35

[a] Calculated using the thermometer of [14].
[b] Mean temperature (°C). In parentheses are the 2 S.D. variation about the mean and number of estimates. 1=Calibration of [7], 2=Calibration of [17].
[c] Error=±25 °C.
[d] Not measured. Variation in this parameter from 0.1 to 0.5 does not change the T estimate beyond its associated error.

rature constraints on the growth of zone-3 monazite. What is more, this suggests that these zones grew during the initial stages of decompression and retrograde replacement of garnet at the end of each metamorphic event. For sample DG167, temperatures considerably lower than peak were generated (271–455 °C), indicating the high-Y rim (zone-2) of monazite in this sample did not grow in equilibrium with matrix xenotime, and hence grew on the prograde P–T path before decompression.

8.3. Monazite–garnet thermometry

As with the application of monazite–xenotime thermometry, it is critical that monazite–garnet thermometry is applied to *equilibrium* pairs of

monazite and garnet. The textural and chemical study outlined above provides the perfect framework in order to accomplish this. What is more, internal consistency between this absolute method and the pseudosection approach will strengthen the confidence in both methodologies. Without such an understanding of monazite and garnet petrogenesis, we caution the use of this thermometer. Further guidelines can be found in [8].

In contrast to monazite–xenotime and xenotime–garnet thermometery, the monazite–garnet thermometer is based on a net transfer reaction. It is required that the anorthite content of plagioclase, the OH content of apatite, the grossular and Y content of garnet, the Y content of monazite, the fugacity of H_2O, and the pressure is known in order to calculate a temperature [8]. The calculated temperature however is most sensitive to the chosen Y content of monazite and garnet. Uncertainties in the other parameters do not tend to move the estimate outside of the ± 25 °C errors associated with the thermometer [8]. Table 2 lists the compositions used, the results, and assumptions made for each sample.

8.4. K98-6

Temperature estimates for the garnet core and monazite zone-1 are in good agreement with the estimates provided by the pseudosection and garnet–xenotime thermometry (~550 °C; see Fig. 3a), and suggest zone-1 monazite (and garnet core) grew at 553 ± 25 °C (at P=6 kbar). Use of an average of zone-2 monazite and the low-Y garnet rim (120 ppm Y) results in a temperature of 585 ± 25 °C (at P=6 kbar), again consistent with the pseudosection approach. As we will demonstrate in the next section, zone-2 monazite in this sample appears to grow over a protracted period of time; hence, the maximum and minimum temperature estimates for this zone may reflect the temperature evolution over this time. The lowest temperature attained is 575 °C and the highest is 592 °C.

8.5. DG136

The pseudosections for DG136 provide well-constrained P–T fields for monazite growth. Monazite is present in the extreme rim of garnet, rim-wards of the

Y annuli, and as such we use a garnet Y content of 90 ppm for both T estimates (Table 2). Although we did not directly measure the Y content of the rim, this value is consistent with the Y X-ray map shown in Fig. 2d, and the LA-ICPMS analyses shown in Fig. 2f. Fig. 3b shows the results of the garnet–monazite thermometer along with the summarised pseudosection for this sample. We noted previously that zone-1 monazite grew during the initial phase of kyanite growth. Fig. 3b indicates that the temperature estimate for zone-1 monazite, that is also consistent with this textural requirement (the grey field in Fig. 3b), is at pressures of ≥ 9 kbar and a temperature of 569 ± 25 °C (or slightly lower at higher pressure; Fig. 3b). The growth of zone-2 monazite is also associated with further kyanite growth. This requirement also helps constrain the P–T of this phase of monazite growth to ≥ 8 kbar and 632 ± 25 °C (or slightly lower at higher pressure).

8.6. DG167

As we will demonstrate in the next section, zone-1 monazite in this sample grows over a protracted period of time; maximum and minimum temperature estimates are therefore relevant here, rather than averages. We assume that both monazite zones grew in equilibrium with primary low-Y garnet (~60 ppm Y; Table 2). The monazite–garnet thermometer gives temperatures from 595 to 611 °C for zone-1 monazite and 642 °C for zone-2 monazite (all calculated at 7 kbar). An agreement with the pseudosection estimates (625 to 665 °C) is possible when the errors associated with this approach (± 25 °C) are taken into account. It is also important to note this pseudosection was drawn without correcting for the effect of garnet growth on the effective bulk composition, which will slightly affect the accuracy of the pseudosection approach.

9. LA-MC-ICPMS U–Pb results

Guided by the Y X-ray maps, monazites in all three samples were analysed for U–Pb in petrographic thin section using LA-MC-ICPMS. Either line rasters $80 \times 18 \times 5$ μm or box rasters $25 \times 45 \times 6$ μm (x, y, z) were used. This flexibility of targeting domain, and

the limited penetration in the z direction, ensured that in most cases only zones imaged in the x and y dimension were analysed. The results of this LA-MC-ICPMS U–Pb investigation are plotted in Fig. 4 and listed in the Table A2 in the EPSL online background data set, associated with this contribution. With reference to the age of particular Y zones, each sample will now be discussed in turn. All errors are quoted at the 2σ level of precision. Where an age is quoted with an associated error this is either a concordia age [29] or the $^{206}Pb/^{238}U$ age of a concordant analysis. The closure temperature for Pb loss by volume diffusion in monazite is controversial, on the basis of laboratory experiments estimates range from ~600 [30] to ~1000 °C [31] for a 100-μm grain and a cooling rate of 10 °C/Ma. Natural examples favour limited Pb diffusion even at temperatures ≥800 °C [32]. Given the peak temperature estimates for these samples (~600 to ~750 °C), we assume that insignificant amounts of Pb have been lost by volume diffusion and that all ages are growth ages. We also

assume that given our careful targeting and compositional mapping, in addition to our ability to resolve mixing in the data (see [20]), measured ages relate to the growth age of the targeted zone only, unless stated otherwise. Given the errors associated with each individual analyses, the effect of unsupported ^{206}Pb from ^{230}Th decay [15] can largely be ignored. However, where concordia ages have been generated, particularly when the quoted error is less than 1–2 Ma, it may be possible that excess ^{206}Pb is sufficient to bias the age to older values. Notably, this effect is unlikely to result in errors greater than 1–2 million years [15].

9.1. K98-6

In order to supplement the data listed in [10], three monazite inclusions and two matrix grains were analysed in situ for U–Pb. The three monazite inclusions are all concordant at ~82 Ma with a concordia age of 81.9 ± 1.0 Ma (MSWD=1.4;
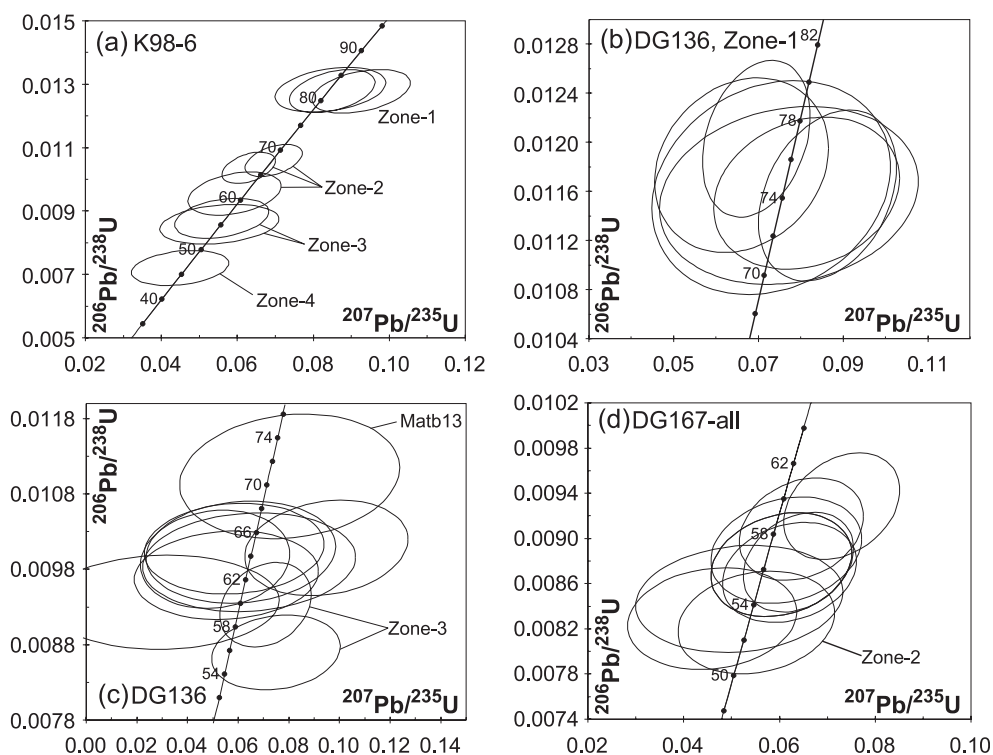

Fig. 4. LA-MC-ICPMS U–Pb data for samples (a) K98-6, (b) DG136 zone-1, (c) DG136 zone-2 and zone-3, and (d) DG167-all. Also labelled are analyses that are discussed further in the text. In (c), only zone-3 analyses are labelled. In (d), only zone-2 analyses are labelled.

Fig. 4a). One line raster on matrix grain matD indicates that zone-2 monazite in this grain is 61.2±3.8 Ma, two analyses of zone-3 monazite have $^{206}Pb/^{238}U$ ages of 55.1±3.2 and 56.3±3.2 Ma (Figs. 1b and 4a). One analysis of zone-4 in this monazite is concordant at 46.2±2.9 Ma. Two line rasters targeted at zone-2 in grain matE give concordant ages of 67.9±2.7 and 66.5±2.6 Ma. This data agrees well with Foster et al. [10] who suggested that zone-1 monazite was ~87 Ma and the zone-2 monazite varied in age from ~66 to ~59 Ma.

9.2. DG136

Thirteen analyses of one large (~500 μm) monazite, and three analyses of the zone-1 portions of three separate matrix monazites (including MatD1 which is included in kyanite) were carried out (Figs. 1d,e,f and 4b,c). In total, six analyses targeted zone-1 monazite, all are of similar age (~74 to ~77 Ma) and concordant and give a combined concordia age of 75.0±1.4 Ma (MSWD=1.1, probability=0.39). Eight analyses targeted zone-2 monazite; again, all of the analyses are concordant and range in age from ~60 to ~65 Ma, with one analysis (matB13) at ~70 Ma. The time-resolved analysis of MatB13 indicates that probably at least two phases of monazite have been analysed, one is similar to zone-2 and zone-3 monazite, the other up to 120 million years old. If this analysis is omitted, the remaining seven analyses give a concordia age of 63.2±1.5 Ma (MSWD=1.3, probability=0.22). We were only able to target zone-3 monazite on two occasions; these ranged in $^{206}Pb/^{238}U$ age from 55.8±2.6 to 59.9±3.0 Ma.

9.3. DG167

A total of 10 monazite analyses was carried out, two inclusions in garnet and three matrix grains (Fig. 4d; Table A2 in the EPSL online background data set). All the analyses are concordant and spread in age from ~53 to ~59 Ma (Fig. 4d), the youngest age corresponds to an analysis of zone-2 monazite, although it is within error of some zone-1 analyses. These data agree well with that of Foster et al. [10] who analysed zone-1 monazite in grain separates, and reported a spread in age from ~55 to ~60 Ma. The data

presented here are consistent with the conclusions of [10] that monazite in this sample grew over a protracted period of around 4–8 million years.

10. P–T–t paths for samples K98-6, DG136, and DG167

In this section, we combine the accessory mineral thermobarometric information with the age data to generate prograde P–T–t paths and estimates of the rate of heating (Fig. 5). Unfortunately, estimates of the associated pressure changes are too imprecise to generate accurate burial rates. Nonetheless, the data presented here provide a near-complete picture of the thermal history of these samples during Cretaceous–Tertiary orogenesis. In the following section, we also place these data in the context established by published geochronological data for these regions and show how they fit into the established regional P–T–t framework.

10.1. K98-6

The metamorphism in the area of the Asian Himalaya from which K98-6 was collected exhibits a relatively complex polymetamorphic thermal history, punctuated by several ductile and semiductile deformation events [12]. This polymetamorphic history is not reflected in the data for K98-6. We find that the first phase of monazite formation occurred at 553±25 °C and ≤6 kbar, during the early stages of garnet growth, at 81.9±1.0 Ma. This coincides well with the timing of closure of the Shyok Suture (the suturing of the Kohistan–Ladakh Island Arc to Asia) at ~90 Ma, thought to be responsible for the earliest deformation fabrics in the Hunza Metamorphic and Plutonic Units [12]. A further period of monazite growth occurred at a slightly higher temperature than the first phase (from 576 to 593 °C), but several million years later, from ~66 to ~59 Ma, reflecting an extended period of heating. Monazite grows once again at ~55.5 Ma, this time during xenotime formation following garnet breakdown during decompression from a peak P–T of 624±25 °C and 4–6 kbar, coincident with the timing of Indo-Asian collision at 65–55Ma [33,34]. Sample K98-6 also melted at 53–56 Ma as indicated by the U–Th–Pb
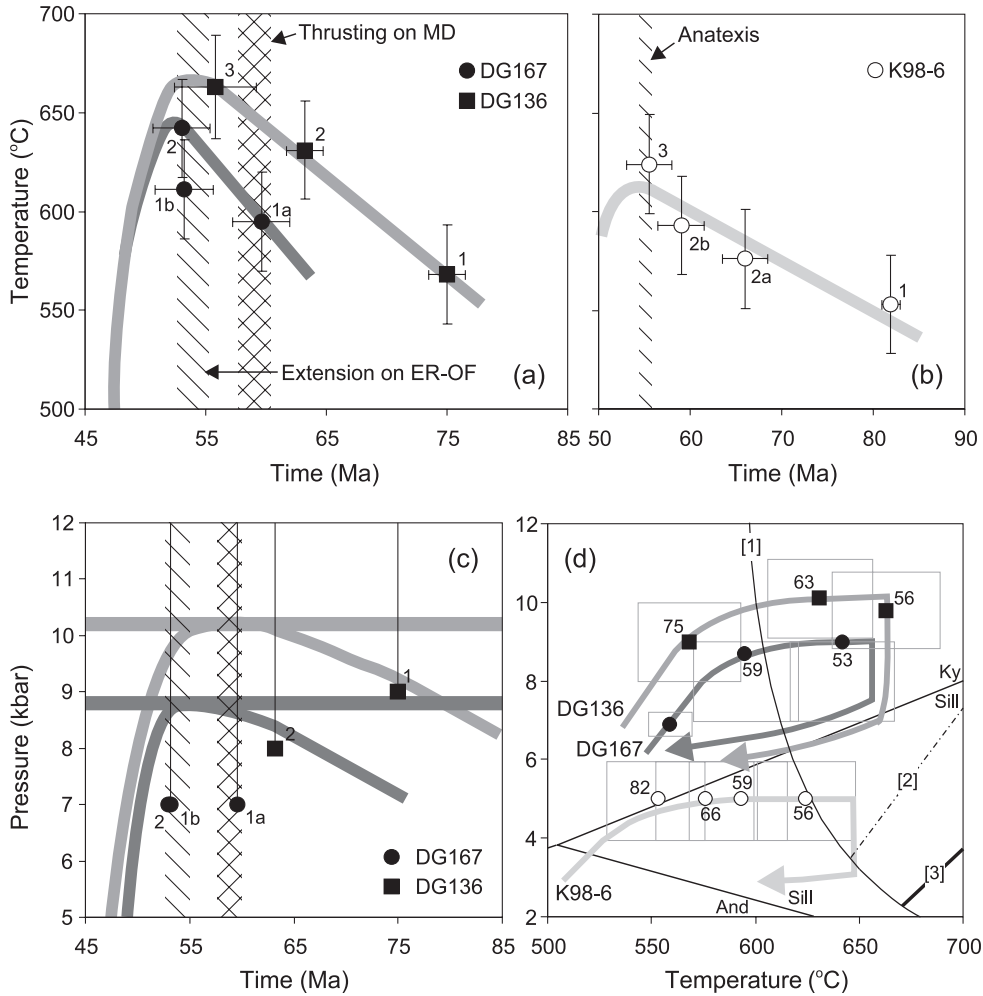
Fig. 5. (a and b) Temperature–time and (c) pressure–time data for samples K98-6, DG136, and DG167. In (a), (b), and (c), the numerical labels denote which monazite zone the estimate relates to. In (a) and (c), the hatched band indicates the minimum timing for extension along the Okanagan-Eagle River Fault System, the cross-hatched band shows the time that thrusting ceased on the Monashee Decollement [37,38]. In (a) and (c), the retrograde portion of the T–t and P–t path is constrained by the cooling data of [39] and Archibald and Journeay (unpublished data cited in [38]). In (b), the hatched band indicates the timing of anatexis in K98-6 as determined by [12]. In (c), pressure is only poorly constrained and minimum estimates are shown as filled squares and circles. The horizontal bands correspond to the peak pressure for each sample. (d) P–T–t paths for samples K98-6, DG136, and DG167. Symbols and colouring as (a) to (c). Symbols (labelled with approximate age in Ma) and light grey squares show P–T–t estimates and associated errors. Line [1] is the wet melting solidus of [35], lines [2] and [3] are the muscovite dehydration solidi of [34,48], respectively. Also shown is the aluminosilicate triple junction, abbreviations as [47]. Note that the pressure is only poorly constrained.

analysis of anatectic monazite [12]. The coincidence in time between the anatectic event and the age of decompression deduced here suggests that the melting was also a consequence of decompression through crossing the muscovite-dehydration solidus. Fig. 5d shows that, given the errors associated with the P–T estimates, it is possible for the P–T path to intersect

the muscovite dehydration solidus of [35]. However, if water activity was close to unity, Fig. 5d also indicates melting may have also occurred at this time due to crossing the wet solidus of [36].

The final phase of monazite growth (zone-4) in K98-6 occurred at ~46 Ma at undetermined metamorphic conditions. Approximately 8 km south (~16

km structural thickness) Fraser et al. [12] note that sillimanite grade monazite growth occurred at 44 ± 2 Ma. This late stage monazite probably represents the distal effects of this event, despite the cessation of deformation in the area at 50–52 Ma [12].

This T–t and P–T–t path is illustrated in Fig. 5b and d. By fitting a linear regression through the T–t data, we can calculate a heating rate of 2.4 ± 1.2 °C/ Ma at a 95% level of confidence (MSWD=1.3).

10.2. DG136 and DG167

The timing of thrusting and extension within the Monashee complex has been relatively well constrained through the dating of crosscutting relationships [37,38]. This work indicates that thrusting along the Monashee Decollement had ceased by ~58 Ma, and exhumation along the Columbia River (CR) and Okanagan-Eagle River (O-ER) normal fault systems had begun at 54–60 Ma, coinciding with the cooling of the complex to 300–500 °C at 45–55 Ma ([39]; Archibald and Journeay, unpublished data cited in [38]). The data presented here agree with and expand this established geological history.

The first period of monazite growth in DG136 occurred during the formation of kyanite and after substantial amounts of garnet growth, at 568 ± 25 °C and ≥9 kbar. A number of in situ U–Pb analyses indicate this growth occurred at 75.0 ± 1.4 Ma. Further monazite formation occurred at 63.2 ± 1.5 Ma, following additional kyanite growth, at 632 ± 25 °C and at pressures ≥8 kbar. The final stage of monazite growth occurred during decompression dated by the youngest zone-3 monazite analysis at 55.8 ± 2.6 Ma. Peak temperature and pressure were probably reached immediately prior to this time.

Zone-1 monazite in sample DG167 appears to have grown over a protracted period of time from ~59 to ~53 Ma. Monazite–garnet thermometry suggests this phase of growth occurred from 595 ± 25 to 611 ± 25 °C, and textures suggest it occurred after kyanite had entered the assemblage, probably at pressures ≥7 kbar. Further monazite growth occurred at 642 ± 25 °C at 53.0 ± 2.4 Ma. Peak P–T was reached shortly after this later monazite growth. Replacement textures, including the growth of xenotime from garnet, suggest metamorphism was terminated by decompression.

Fig. 5a, c and d shows the T–t, P–t, and P–T–t paths, respectively, for these samples. Once again, pressure estimates at the time of monazite growth are imprecise, although we can say that both samples were at elevated pressures prior to the growth of zone-1 monazites. For sample DG167, we can also estimate the post-garnet-growth P–T path with some confidence (Fig. 5d). The P–T–t paths for both samples suggest there was little burial following monazite growth (Fig. 5d). Given that these samples were buried in part by movement on the Monashee Decollement [11], these data constrain the initiation of thrusting to prior to 75 Ma, and suggest it had ceased by ~55 Ma (Fig. 5), consistent with the data of [38]. The T–t paths are similar and linear, allowing heating rates to be determined using a linear regression. The errors and limited spread of the data for DG167 only allow a relatively poor estimate of heating rate at 7 ± 6 °C/Ma (using the lowest zone-1 T–t and the zone-2 T–t), which is consistent with the better constrained estimate of 5 ± 2 °C/Ma (MSWD=0.1) for sample DG136. In both cases, the errors are quoted at a 95% confidence level. If the peak P–T estimate is used to determine the growth temperature of zone-3 monazite in DG136, instead of monazite–xenotime thermometry, the heating rate is no longer constant and it is required that the heating rate increased to 13 ± 8.1 °C/Ma some time after ~64 Ma. Although the data for DG167 are consistent with this increase, we find the estimate based on the [7] calibration of the monazite–xenotime thermometer to be more satisfactory and use a heating rate of 5.0 ± 2.0 °C/Ma.

Metamorphism in both samples was terminated by decompression dated at 55.5 ± 2.6 Ma in DG136 and after 53.0 ± 2.4 Ma in DG167. This is a minimum estimate for DG167 since monazite zone-2 in this sample grew on the prograde P–T path. The possibility therefore exists that sample DG136 was being exhumed while DG167 was still undergoing burial and heating (Fig. 5d). However, in the absence of better age constraints, we make this interpretation with caution. Nonetheless, the timing of exhumation deduced here (55–53 Ma) is consistent with published estimates for cooling to 300–500 °C and the timing of extension on the CRF and O-ERF ([39]; Archibald and Journeay, unpublished data cited in [38]).

A more complete discussion of the regional geological significance of these data is beyond the scope of this contribution. Our aim here is simply to demonstrate that this approach yields data fully compatible with the established geological history of these two areas, and that such data can make a significant contribution towards solving geological problems.

11. Broader implications

Although the data set presented here is limited, it does provide valuable insights into the mechanisms of prograde metamorphism. It is noteworthy that these data provide heating rates, P–T–t paths, peak P–T and durations of metamorphism that are of similar magnitude to those predicted by 2D thermal models (e.g., [40]) and to those reconstructed using other methods (e.g., garnet dating; [5]). However, these same thermal models highlight the importance of a number of parameters, such as burial rate (e.g., [40]), the rate of internal radiogenic heat production, upper crustal thickness (e.g., [41]), and initial geothermal gradient (e.g., [40]), in determining the character of prograde metamorphism. Because these parameters are likely to vary between orogenic belts, it is perhaps surprising then that the P–T–t paths for the Omineca Belt, the Asian Himalaya, and those of other recent mountain belts (e.g., the Indian Himalaya; [5,18]) are so similar. This observation suggests that either the parameters that control the nature of prograde metamorphism are less variable than previously thought (e.g., upper crustal thickness and composition may not vary significantly, especially between recent continental collision zones), or the interdependency of the parameters is such that heating rate and burial rate during orogenesis are self-limiting. Perhaps due to a thermo-rheological effect, for example, [42] highlights the importance of prograde melt generation in the lower crust in determining the duration and style of metamorphism in the upper crust.

These data also have a bearing on the debate of the causes of the inverted metamorphic field gradient that characterises the footwall of the Monashee Decollement and is a common feature of the footwalls of many other crustal-scale thrust sheets. The peak P–T for DG167 is a maximum of 3.8 kbar (≈ 12 km) and

110 °C *lower* than DG136; our P–T–t paths suggest this difference was maintained throughout their prograde evolution (Fig. 5). This is a significant observation because DG136 crops out in the immediate footwall of the Monashee Decollement ~1.5 km structurally *above* DG167. We therefore suggest that the inverted metamorphic gradient that characterises the Monashee complex is not a consequence of the prograde evolution (as suggested by, e.g., [37] and references therein), but instead relates to the processes and mechanisms of exhumation (supporting the arguments of [11]). Further studies of this kind are however required to confirm whether this mechanism for the generation of inverted metamorphic field gradients is applicable to other regions.

12. Conclusions

From the data presented here, we deduce a near-complete picture of the prograde P–T–t history of three samples buried and metamorphosed during Cretaceous–Tertiary collisional orogenesis, allowing timing constraints to be placed on prograde events and heating rates. The approach followed here, where the episodic growth of monazite is exploited using novel techniques and methodologies to construct prograde P–T–t points, will, over the next couple of years, be achievable in a number of laboratories, thanks to the proliferation of in situ dating techniques, such as LA-qudrapole-ICPMS [43] and LA-MC-ICPMS [20], in addition to mini-XRF [44], EMP [45], and ion probe [46]. However, we stress that in order to achieve the most out of in situ dating methodologies, a full textural and compositional study of the analysed grains must be performed prior to age analysis.

Appendix A. Supplementary data

Supplementary data associated with this article can be found, in the online version, at doi:10.1016/j.epsl.2004.09.024.

References

[1] D. Vance, W. Muller, I.M. Villa, Geochronology: linking the isotopic record with petrology and textures—an introduction, in: D. Vance, W. Muller, I.M. Villa (Eds.), Geochronology: Linking the Isotopic Record with Petrology and Textures, Geol. Soc. London, Spec. Publ. 220 (2003) 25–47.

[2] P.C. England, A.B. Thompson, Pressure–temperature–time paths of regional metamorphism: I. Heat transfer during the evolution of regions of thickened crust, J. Petrol. 25 (1984) 894–928.

[3] R.A. Jamieson, C. Beaumont, P. Fullsack, B. Lee, Barrovian regional metamorphism: where's the heat, in: P.J. Treloar, P.J. O'Brien (Eds.), What Drives Metamorphism and Metamorphic Reactions? Spec. Publ. Geol. Soc. London 138 (1998) 23–51.

[4] A.I. Chemenda, J.P. Burg, M. Mattauer, Evolutionary model of the Himalaya–Tibet system: geopeom based on new modelling, geological and geophysical data, Earth Planet. Sci. Lett. 174 (2000) 397–409.

[5] D. Vance, N. Harris, The timing of prograde metamorphism in the Zanskar Himalaya, Geology 27 (1999) 395–398.

[6] M. Thoni, Sm–Nd isotope systematics in garnet from different lithologies (Eastern Alps): age results, and an evaluation of potential problems for garnet Sm–Nd chronometery, Chem. Geol. 194 (4) (2003) 353–379.

[7] W. Heinrich, G. Andrehs, G. Franz, Monazite–xenotime miscibility gap thermometry: I. An empirical calibration, J. Metamorph. Geol. 15 (1997) 2–16.

[8] J.M. Pyle, F.S. Spear, R.L. Rudnick, W.F. McDonough, Monazite–xenotime–garnet equilibrium in metapelites and a new monazite–garnet thermometer, J. Petrol. 42 (11) (2001) 2083–2107.

[9] G.L. Foster, R.R. Parrish, Metamorphic monazite and the generation of P–T–t paths, in: D. Vance, W. Muller, I.M. Villa (Eds.), Geochronology: Linking the Isotopic Record with Petrology and Textures, Geol. Soc. London Spec. Publ. 220 (2003) 25–47.

[10] G.L. Foster, H.D. Gibson, R.R. Parrish, M.S.A. Horstwood, J. Fraser, A. Tindle, Textrual, chemical and isotopic insights into the nature and behaviour of metamorphic monazite, Chem. Geol. 191 (2002) 183–207.

[11] H.D. Gibson, R.L. Brown, R.R. Parrish, Deformation-induced inverted metamorphic field gradients: an example from the southeastern Canadian Cordillera, J. Struct. Geol. 21 (1999) 751–767.

[12] J. Fraser, M. Searle, R.R. Parrish, S. Noble, Chronology of deformation, metamorphism and magmatism in the southern Karakoram Mountains, Geol. Soc. Am. Bull. 113 (11) (2001) 1443–1455.

[13] R. Powell, T. Holland, Optimal geothermometry and geobarometry, Am. Mineral. 79 (1994) 120–133.

[14] A. Bhattacharya, L. Mohanty, A. Maji, S.K. Sen, M. Raith, Nonideal mixing in the phlogopite–annite binary—constraints from experimental-data on Mg–Fe partitioning and a reformulation of the biotite garnet geothermometer, Contrib. Mineral. Petrol. 111 (1) (1992) 87–93.

[15] R.R. Parrish, U–Pb dating of monazite and its application to geological problems, Can. J. Earth Sci. 27 (11) (1990) 1431–1450.

[16] D. Vance, E. Mahar, Pressure–temperature paths from P–T pseudosections and zoned garnets: potential, pitfalls and examples from the Zanskar Himalaya, NW India, Contrib. Mineral. Petrol. 132 (1998) 225–245.

[17] R. Gratz, W. Heinrich, Monazite–xenotime thermobarometry: experimental calibration of the miscibility gap in the binary system $CePO_4$–YPO_4, Am. Mineral. 82 (1997) 772–780.

[18] G. Foster, P. Kinny, C. Prince, D. Vance, N. Harris, The significance of monazite U–Th–Pb age data in metamorphic assemblages; a combined study of monazite and garnet chronometry, Earth Planet. Sci. Lett. 181 (2000) 327–340.

[19] J.M. Pyle, F.S. Spear, Four generations of accessory phase growth in low-pressure migmatites from SW New Hampshire, Am. Mineral. 88 (2–3) (2003) 338–351.

[20] M.S.A. Horstwood, G.L. Foster, R.R. Parrish, S. Noble, G.M. Nowell, Common-Pb corrected in situ U–Pb accessory mineral geochronology by LA-MC-ICP-MS, J. Anal. At. Spectrom. 18 (2003) 837–846.

[21] S. Chenery, J.M. Cook, Determination of rare earth elements in single mineral grains by laser ablation microprobe inductively coupled plasma mass spectrometry—preliminary study, J. Anal. At. Spectrom. 8 (1993) 299–303.

[22] R.J. Tracy, Compositional zoning and inclusions in metamorphic minerals, in: J.M. Ferry (Ed.), Characterisation of Metamorphism Through Mineral Equilibria, Reviews in Mineralogy, vol. 10, Minerological Society of America, Washington, 1982, pp. 355–397.

[23] J. Pyle, F.S. Spear, Yttrium zoning in garnet: coupling of major and accessory phases during metamorphic reactions, Geol. Mater. Res. 1 (6) (1999) 1–49.

[24] J.M. Pyle, F.S. Spear, An empirical garnet (YAG)–xenotime thermometer, Contrib. Mineral. Petrol. 138 (2000) 51–58.

[25] A. Lanzirotti, Yttrium zoning in metamorphic garnets, Geochim. Cosmochim. Acta 59 (19) (1995) 4105–4110.

[26] T. Holland, R. Powell, An internally-consistent thermodynamic data set for phases of petrological interest, J. Metamorph. Geol. 16 (1998) 309–343.

[27] T.P. Evans, A method for calculating effective bulk composition modification due to crystal fractionation in garnet-bearing schist: implications for isopleth thermobarometry, J. Metamorph. Geol. 22 (2004) 547–557.

[28] P.C. Engl, S.W. Richardson, The influence of erosion upon the mineral facies of rocks from different metamorphic environments, J. Geol. Soc. (Lond.) 134 (1977) 201–213.

[29] K.R. Ludwig, Users Manual for Isoplot/Ex v.2.3. A Geochronological Toolkit for Microsoft Excel, Berkeley Geochronological Center Special Publication, 1a, 2000, Berkeley, California, 57 pp.

[30] H.A. Smith, B.J. Giletti, Pb diffusion in monazite, Geochim. Cosmochim. Acta 61 (5) (1997) 1047–1055.

[31] D.J. Cherniak, E.B. Watson, M. Grove, T.M. Harrison, Pb diffusion in monazite: a combined RBS/SIMS study, Geochim. Cosmochim. Acta 68 (4) (2004) 829–840.

[32] F.S. Spear, R.R. Parrish, Petrology and cooling rates of the Valhalla Complex, British-Columbia, Canada, J. Petrol. 37 (4) (1996) 733–765.

[33] D.B. Rowley, Age of initiation of collision between India and Asia: a review of stratigraphic data, Earth Planet. Sci. Lett. 145 (1996) 1–13.

[34] C.T. Klootwijk, J.S. Gee, J.W. Peirce, G.M. Smith, P.L. McFadden, An early India–Asia contact—paleomagnetic constraints from Ninetyeast ridge, ODP Leg 121, Geology 20 (5) (1992) 395–398.

[35] P. Petö, An experimental investigation of melting reactions involving muscovite and paragonite in the silica-undersaturated portion of the system K_2O–Na_2O–Al_2O_3–SiO_2–H_2O, Prog. Exp. Petrol. 3 (1976) 41–45.

[36] N. Le Breton, A.B. Thompson, Fluid-absent (dehydration) melting of biotite in metapelites in the early stages of crustal anatexis, Contrib. Mineral. Petrol. 99 (1988) 226–237.

[37] R.R. Parrish, S.D. Carr, D.L. Parkinson, Eocene extensional tectonics and geochronology of the southern Omineca Belt, British-Columbia and Washington, Tectonics 7 (2) (1988) 181–212.

[38] R.R. Parrish, Thermal evolution of the southeastern Canadian Cordillera, Can. J. Earth Sci. 32 (10) (1995) 1618–1642.

[39] R.L. Armstrong, R.R. Parrish, P. Vanderheyden, K. Scott, D. Runkle, R.L. Brown, Earth Proterozoic basement exposures in the southern Canadian Cordillera—core gneiss of Frenchman Cap, unit-I of the Grand-Forks Gneiss, and the Vaseaux Formation, Can. J. Earth Sci. 28 (8) (1991) 1169–1201.

[40] C. Ruppel, K.V. Hodges, Pressure–temperature–time paths from two-dimensional thermal models: prograde, retrograde, and inverted metamorphism, Tectonics 13 (1) (1994) 17–44.

[41] A.D. Huerta, L.H. Royden, K.V. Hodges, The effects of accretion, erosion and radiogenic heat on the metamorphic evolution of collisional orogens, J. Metamorph. Geol. 17 (1999) 349–366.

[42] L. Hollister, The role of melt in the uplift and exhumation of orogenic belts, Chem. Geol. 108 (1993) 31–48.

[43] J. Kosler, M. Tubrett, P. Sylvester, Application of laser ablation ICPMS to U–Th–Pb dating of monazite, Geostand. Newsl. 25 (2–3) (2001) 375–386.

[44] M. Engi, A.K. Cheburkin, V. Koppel, Nondestructive chemical dating of young monazite using XRF: 1. Design of a miniprobe, age data for samples from the Central Alps, and comparison to U–Pb (TIMS) data, Chem. Geol. 191 (1–3) (2002) 225–241.

[45] M.L. Williams, M.J. Jercinovic, M.P. Terry, Age mapping and dating of monazite on the electron microprobe: deconvoluting multistage tectonic histories, Geology 27 (11) (1999) 1023–1026.

[46] T.M. Harrison, K.D. McKeegan, P. Lefort, Detection of inherited monazite in the Manaslu leucogranite by [208]Pb/[232]Th ion microprobe dating: crystallisation age and tectonic implications, Earth Planet. Sci. Lett. 133 (1995) 271–282.

[47] R. Kretz, Symbols for rock-forming minerals, Am. Mineral. 68 (1983) 277–279.

[48] A.E. Patino Douce, N. Harris, Experimental constraints on Himalayan Anatexis, J. Petrol. 39 (4) (1998) 689–710.